
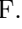
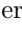
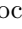

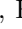



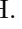
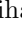

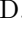




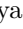





Measurement of Angular Coefficients of $\bar{B} \rightarrow D^* \ell \bar{\nu}_\ell$: Implications for $|V_{cb}|$ and Tests of Lepton Flavor Universality

M. T. Prim , F. Bernlochner , F. Metzner , H. Aihara , D. M. Asner , T. Aushev , R. Ayad , V. Babu , Sw. Banerjee , P. Behera , K. Belous , J. Bennett , M. Bessner , V. Bhardwaj , B. Bhuyan , T. Bilka , D. Biswas , D. Bodrov , A. Bondar , J. Borah , M. Bračko , P. Branchini , T. E. Browder , A. Budano , M. Campajola , L. Cao , D. Červenkov , P. Chang , B. G. Cheon , S.-K. Choi , Y. Choi , S. Choudhury , J. Cochran , S. Das , N. Dash , G. De Nardo , G. De Pietro , R. Dhamija , F. Di Capua , Z. Doležal , T. V. Dong , S. Dubey , P. Ecker , D. Epifanov , T. Ferber , D. Ferlewicz , B. G. Fulsom , R. Garg , V. Gaur , A. Giri , P. Goldenzweig , T. Gu , K. Gudkova , C. Hadjivasiliou , T. Hara , H. Hayashii , S. Hazra , M. T. Hedges , D. Herrmann , M. Hernández Villanueva , W.-S. Hou , C.-L. Hsu , K. Inami , G. Inguglia , N. Ipsita , A. Ishikawa , R. Itoh , M. Iwasaki , W. W. Jacobs , C. Kiesling , C. H. Kim , D. Y. Kim , K.-H. Kim , P. Kodyš , T. Konno , A. Korobov , S. Korpar , E. Kovalenko , P. Krizan , P. Krokovny , T. Kuhr , M. Kumar , R. Kumar , Y.-J. Kwon , T. Lam , S. C. Lee , P. Lewis , L. K. Li , L. Li Gioi , J. Libby , D. Liventsev , Y. Ma , T. Matsuda , D. Matvienko , S. K. Maurya , F. Meier , M. Merola , K. Miyabayashi , R. Mizuk , G. B. Mohanty , I. Nakamura , M. Nakao , D. Narwal , Z. Natkaniec , A. Natochii , L. Nayak , S. Nishida , H. Ono , P. Oskin , P. Pakhlov , G. Pakhlova , S.-H. Park , A. Passeri , S. Patra , T. K. Pedlar , R. Pestotnik , L. E. Piilonen , T. Podobnik , E. Prencipe , M. Röhrken , N. Rout , G. Russo , S. Sandilya , L. Santelj , V. Savinov , P. Schmolz , G. Schnell , C. Schwanda , Y. Seino , K. Senyo , W. Shan , J.-G. Shiu , J. B. Singh , E. Solovieva , M. Starič , Z. S. Stottler , M. Sumihama , M. Takizawa , K. Tanida , F. Tenchini , R. Tiwary , K. Trabelsi , Y. Unno , S. Uno , P. Urquijo , Y. Usov , S. E. Vahsen , K. E. Varvell , A. Vossen , M.-Z. Wang , X. L. Wang , E. Won , B. D. Yabsley , W. Yan , S. B. Yang , J. H. Yin , L. Yuan , Z. P. Zhang , V. Zhilich , and V. Zhukova

(The Belle Collaboration)

We measure the complete set of angular coefficients J_i for exclusive $\bar{B} \rightarrow D^* \ell \bar{\nu}_\ell$ decays ($\ell = e, \mu$). Our analysis uses the full 711 fb^{-1} Belle data set with hadronic tag-side reconstruction. The results allow us to extract the form factors describing the $B \rightarrow D^*$ transition and the Cabibbo-Kobayashi-Maskawa matrix element $|V_{cb}|$. Using recent lattice QCD calculations for the hadronic form factors, we find $|V_{cb}| = (41.0 \pm 0.7) \times 10^3$ using the BGL parameterization, compatible with determinations from inclusive semileptonic decays. We search for lepton flavor universality violation as a function of the hadronic recoil parameter w , and investigate the differences of the electron and muon angular distributions. We find no deviation from Standard Model expectations.

In this Letter, we present the first determination of the full set of angular coefficients describing the full differential decay rate of exclusive semileptonic $\bar{B} \rightarrow D^* \ell \bar{\nu}_\ell$ ($\ell = e, \mu$) decays. Our analysis uses the complete Belle data set, with an integrated luminosity of 711 fb^{-1} at the $\Upsilon(4S)$ resonance. The data set was recorded at the KEKB e^+e^- collider [1] by the Belle detector. Belle is a large-solid-angle magnetic spectrometer. A detailed description of its performance and subdetectors can be found in Ref. [2]. We use hadronic tagging to reconstruct the accompanying B meson. The measured angular coefficients allow us to determine the form factors that describe the non-perturbative dynamics describing the $B \rightarrow D^*$ transition and consequently, in conjunction with information from Lattice QCD (LQCD), to extract the Cabibbo-Kobayashi-Maskawa (CKM) matrix element $|V_{cb}|$. The angular coefficients are also sensitive to beyond Standard Model (SM) effects and are used to test lepton flavor universality. Our measurement is based on the same dataset analyzed in a previous publication [3], which focused on partial branching fractions in bins of

the hadronic recoil parameter

$$w = \frac{m_B^2 + m_{D^*}^2 - q^2}{2m_B m_{D^*}}, \quad (1)$$

with the B (D^*) mass m_B (m_{D^*}) and the momentum-transfer squared to the lepton-neutrino system q^2 , and the decay angles θ_ℓ , θ_V , and χ . The decay angles are defined as follows: θ_ℓ is the angle between the lepton and the direction opposite the B meson in the virtual W -boson rest frame, θ_V is the angle between the D meson and the direction opposite the B meson in the D^* rest frame, and χ is the angle between the two decay planes spanned by the $W^+ - \ell$ and $D^* - D$ systems in the B meson rest frame. The analysis strategy closely follows the methodology outlined in Ref. [3], with modifications to facilitate the measurement of angular coefficients as a function of w .

The four-dimensional differential decay rate for $\bar{B} \rightarrow D^* \ell \bar{\nu}_\ell$ can be expressed in terms of 12 functions $J_i = J_i(w)$, which only depend on w , as

$$\begin{aligned}
\frac{d\Gamma(\bar{B} \rightarrow D^* \ell \bar{\nu}_\ell)}{dw d\cos\theta_\ell d\cos\theta_V d\chi} &= \frac{2G_F^2 \eta_{EW}^2 |V_{cb}|^2 m_B^4 m_{D^*}}{2\pi^4} \times \left(J_{1s} \sin^2 \theta_V + J_{1c} \cos^2 \theta_V \right. \\
&+ (J_{2s} \sin^2 \theta_V + J_{2c} \cos^2 \theta_V) \cos 2\theta_\ell + J_3 \sin^2 \theta_V \sin^2 \theta_\ell \cos 2\chi \\
&+ J_4 \sin 2\theta_V \sin 2\theta_\ell \cos \chi + J_5 \sin 2\theta_V \sin \theta_\ell \cos \chi + (J_{6s} \sin^2 \theta_V + J_{6c} \cos^2 \theta_V) \cos \theta_\ell \\
&\left. + J_7 \sin 2\theta_V \sin \theta_\ell \sin \chi + J_8 \sin 2\theta_V \sin 2\theta_\ell \sin \chi + J_9 \sin^2 \theta_V \sin^2 \theta_\ell \sin 2\chi \right). \quad (2)
\end{aligned}$$

The expression depends on Fermi's coupling constant G_F , the electroweak correction η_{EW} [4], the CKM matrix element V_{cb} , and the masses of B (m_B) and D^* (m_{D^*}) mesons.

We determine the angular coefficients in bins of w , $\bar{J}_i = \int_{\Delta w} J_i(w) dw$, from experimental data with the definition from Ref. [5]:

$$\bar{J}_i = \frac{1}{N_i} \sum_{j=1}^8 \sum_{k,l=1}^4 \eta_{i,j}^\chi \eta_{i,k}^{\theta_\ell} \eta_{i,l}^{\theta_V} R_{jkl}. \quad (3)$$

The normalization factor N_i stems from trigonometric integrals. The angles θ_ℓ , θ_V , and χ are divided into bins of size $\pi/4$. The weight factors $\eta_{i,n}^\alpha$ with $\alpha \in \{\chi, \theta_\ell, \theta_V\}$ are given in Ref. [5] and the product of these factors define a specific phase-space bin where signal is extracted. The factor R_{jkl} represents the partial rate in the corresponding phase-space bin jkl . We combine phase-space bins with identical products of the weights $\eta_{i,n}^\alpha$ during signal extraction, resulting in yields of total 36 merged bins to obtain 12 J_i coefficients using Eq. (3) in each bin of w . In the limit of massless charged leptons, the angular coefficient J_{6c} vanishes. Furthermore, the angular coefficients J_7 , J_8 , and J_9 are zero within the SM of particle physics, only contributing to scenarios involving new physics.

We reconstruct two B meson candidates, a tag B and a signal B . Signal B meson candidates are reconstructed as follows: We consider both charged and neutral B mesons with the decay chains $\bar{B}^0 \rightarrow D^{*+} \ell \bar{\nu}_\ell$, $D^{*+} \rightarrow D^0 \pi^+$, $D^{*+} \rightarrow D^+ \pi^0$, and $B^- \rightarrow D^{*0} \ell \bar{\nu}_\ell$ with $D^{*0} \rightarrow D^0 \pi^0$ [6].

To select charged tracks, we apply the following criteria: $dr < 2$ cm and $|dz| < 4$ cm, where dr is the impact parameter perpendicular to the beam-axis and with respect to the interaction point and dz is the z coordinate along the beam-axis of the impact parameter. Tracks are also required to have transverse momenta $p_T > 0.1$ GeV/c. In addition, we utilize particle identification subsystems to identify electrons, muons, charged pions, kaons, and protons. Electron (muon) tracks are required to have momenta in the lab frame $p^{\text{Lab}} > 0.3$ GeV/c ($p^{\text{Lab}} > 0.6$ GeV/c). The momenta of particles identified as electrons are corrected for bremsstrahlung by including photons within a 2° cone defined around the electron momentum at the point of closest approach to the interaction point (IP).

Photon selection criteria are based on their energies:

$E_\gamma > 100$ MeV for the forward endcap ($12^\circ < \theta < 31^\circ$), 150 MeV for the backward endcap ($132^\circ < \theta < 157^\circ$), and 50 MeV for the barrel region ($32^\circ < \theta < 129^\circ$) of the calorimeter. π^0 candidates are formed from pairs of photons with invariant mass within the range of 104 MeV/c² to 165 MeV/c². The difference between the reconstructed π^0 mass and the nominal mass ($m_{\pi^0} = 135$ MeV/c² [7]) must be smaller than three times the estimated mass resolution.

K_S^0 mesons are reconstructed from oppositely charged track pairs within a reconstructed invariant mass window of 398 MeV/c² to 598 MeV/c² and selected with a multivariate method. For details on the multivariate method used, see Ref. [8]. The reconstructed K_S^0 mass has to differ from the nominal value ($m_{K_S^0} = 498$ MeV/c² [7]) by less than 3σ of the estimated mass resolution.

We reconstruct the following decays of the D mesons: $D^+ \rightarrow K^- \pi^+ \pi^+$, $D^+ \rightarrow K^- \pi^+ \pi^+ \pi^0$, $D^+ \rightarrow K^- \pi^+ \pi^+ \pi^+ \pi^-$, $D^+ \rightarrow K_S^0 \pi^+$, $D^+ \rightarrow K_S^0 \pi^+ \pi^0$, $D^+ \rightarrow K_S^0 \pi^+ \pi^+ \pi^-$, $D^+ \rightarrow K_S^0 K^+$, $D^+ \rightarrow K^+ K^- \pi^+$, $D^0 \rightarrow K^- \pi^+$, $D^0 \rightarrow K^- \pi^+ \pi^0$, $D^0 \rightarrow K^- \pi^+ \pi^+ \pi^-$, $D^0 \rightarrow K^- \pi^+ \pi^+ \pi^- \pi^0$, $D^0 \rightarrow K_S^0 \pi^0$, $D^0 \rightarrow K_S^0 \pi^+ \pi^-$, $D^0 \rightarrow K_S^0 \pi^+ \pi^- \pi^0$, and $D^0 \rightarrow K^- K^+$. We apply a decay-channel-optimized mass window selection to the D meson candidates. The π^0 daughters from D meson candidates are required to have center-of-mass momenta $p_{\pi^0}^{\text{CMS}} > 0.2$ GeV/c, except for the decay $D^0 \rightarrow K^- \pi^+ \pi^+ \pi^- \pi^0$ where this criterion is not applied. To reduce combinatorial background, the reconstructed D mesons within an event are ranked based on the absolute difference between the reconstructed mass and the nominal mass ($m_{D^+} = 1.870$ GeV/c², $m_{D^0} = 1.865$ GeV/c² [7]), and up to ten candidates with the smallest mass difference are selected.

D^* mesons are reconstructed in three decay channels: $D^{*0} \rightarrow D^0 \pi_{\text{slow}}^0$, $D^{*+} \rightarrow D^+ \pi_{\text{slow}}^0$, and $D^{*+} \rightarrow D^0 \pi_{\text{slow}}^+$. Charged slow pions must have a center-of-mass momentum below 0.4 GeV/c, and the mass difference between the reconstructed masses M_X of the D^* and D candidates $\Delta M = M_{D^*} - M_D$ has to be smaller than 0.155 GeV/c² (0.160 GeV/c²) for D^{*+} (D^{*0}) mesons.

Signal- B meson candidates are reconstructed by combining selected D^* candidates and a lepton candidate. The loose selection $1 \text{ GeV}/c^2 < M_{D^* \ell} < 6 \text{ GeV}/c^2$ is applied to reduce combinatorial background.

We perform global-decay-chain vertex fitting using

TreeFitter [9]. Events that cannot be successfully fitted are rejected.

Tag- B meson candidates are reconstructed using the Full Event Interpretation (FEI) [10] algorithm. The algorithm fully reconstructs B mesons in 36 B -decay modes. Selection criteria include the requirement $M_{bc}^{\text{tag}} = \sqrt{s/2 - \vec{p}_{\text{tag}}^2} > 5.27 \text{ GeV}/c^2$, $\Delta E_{\text{tag}} = E_{\text{tag}} - \sqrt{s}/2 \in [-0.15, 0.10] \text{ GeV}$, where $p_{\text{tag}} = (E_{\text{tag}}, \vec{p}_{\text{tag}})$ is the 4-momentum of the B_{tag} meson in the center-of-mass frame, and the probability of the classifier for the tag-candidate $\mathcal{P}_{\text{FEI}} > 10^{-3}$. We form an $\Upsilon(4S)$ candidate from combinations of tag- and signal- B mesons, requiring that there are no additional charged particles in the event. The reconstructed invariant mass of the $\Upsilon(4S)$ candidate is limited to $M_{\Upsilon(4S)} \in [7.0, 13.0] \text{ GeV}/c^2$.

Non-resonant e^+e^- interactions are suppressed using event shape variables: The magnitude of the thrust of the full event [11], the angle between the thrust axis of the tag- B and the beamline, the angle between the thrust axes of the two B mesons [11], the reduced Fox-Wolfram moment R_2 [11], the modified Fox-Wolfram moments [12], and the CLEO Cones [13]. These variables are combined using a multivariate classifier based on gradient boosted decision trees [14].

The average number of $\Upsilon(4S)$ candidates is 4.3. In events with more than one candidate we retain only the candidate with the lowest E_{ECL} , the sum of unassigned photon clusters in the full event reconstruction. If multiple candidates remain, the one with the smallest $|\Delta E_{\text{tag}}|$ is chosen. If a conclusive selection cannot be made, a random candidate is selected.

The angular coefficients are extracted in four bins of w . In each w bin, we determine the signal yield in bins of the decay angles θ_ℓ , θ_V , and χ , defined in Equation 3. The signal yield in the bins of 36 angles \times 4 w bins \times 4 decay modes is determined using the M_{miss}^2 distribution, where $M_{\text{miss}}^2 = (p_{e^+e^-} - p_{\text{tag}} - p_{D^*} - p_\ell)^2$. A binned maximum likelihood fit is performed using Monte-Carlo (MC) simulations to determine template shapes for signal and background events. Nuisance parameters account for systematic effects on the shapes of the templates in the fit. The M_{miss}^2 distribution is binned into five bins to reduce dependence on the modelling of the M_{miss}^2 resolution. The statistical correlation of the partial rates in different phase-space regions projected onto M_{miss}^2 is determined by bootstrapping.

The determined signal yields are transformed into partial rates $\Delta\Gamma/\Delta x$ through a process of unfolding, utilizing the matrix inversion method, and subsequent correction for efficiency. A more detailed description of the individual steps can be found in Ref. [3]. Unfolding is necessary to correct for resolution effects causing migration of signal events into different regions of phase-space. Systematic uncertainties in the migration matrix and efficiency correction are accounted for by reweighting the simulated events. The most significant source of systematic uncertainty is from the limited available MC sam-

ple size used to derive migration matrices and efficiency corrections. Smaller uncertainties arise from D decay branching fractions [7], assumptions about $B \rightarrow D^* \ell \bar{\nu}_\ell$ form factors [15], the impact of the FEI on the measured shapes, lepton identification efficiency, and the efficiencies for reconstructing tracks, neutral pions, slow pions, and K_S^0 mesons.

Subsequently, the angular coefficients \bar{J}_i are calculated from the $\Delta\Gamma/\Delta x$ using Eq. (3). Due to the challenges in calibrating the absolute efficiency of the FEI, we quote normalized angular coefficients $\hat{J}_i = J_i/\mathcal{N}$, with $\mathcal{N} = \frac{8}{9}\pi \sum_{i=0}^{w\text{bins}} 3\bar{J}_{1c}^{(i)} + 6\bar{J}_{1s}^{(i)} - \bar{J}_{2c}^{(i)} - 2\bar{J}_{2s}^{(i)}$ summing over the four w bins.

The analysis is validated using Asimov data and pseudo-experiments, for which we see no biases in central values or uncertainties. The measured normalized angular coefficients \hat{J}_i as a function of w are displayed in Fig. 1.

We calculate the average of the \hat{J}_i determined in the four decay modes, taking into account the correlations and uncertainties. We fit the CLN [16] and BGL [17, 18] form factor parameterizations to the averaged central values of the normalized measured angular coefficients within the SM (i.e. $J_{7,8,9} = 0$) and neglecting electron and muon masses (so that $J_{6c} = 0$). Beyond zero-recoil lattice calculations by the MILC [19], HPQCD [20], and JLQCD [21] groups are included in the fit to constrain the form factors. To obtain $|V_{cb}|$ from the normalized angular coefficients, we use the absolute branching fraction of $\mathcal{B}(\bar{B}^0 \rightarrow D^{*+} \ell \bar{\nu}_\ell) = (5.03 \pm 0.10)\%$. This value is obtained from the branching fractions $\mathcal{B}(B^- \rightarrow D^{*0} \ell \bar{\nu}_\ell) = (5.58 \pm 0.22)\%$, $\mathcal{B}(\bar{B}^0 \rightarrow D^{*+} \ell \bar{\nu}_\ell) = (4.97 \pm 0.12)\%$ [22] and the lifetimes $\tau_{\bar{B}^0} = 1.520 \text{ ps}$ and $\tau_{B^-} = 1.638 \text{ ps}$ [7], assuming isospin symmetry.

The fit is performed by minimizing the χ^2 function defined as

$$\begin{aligned} \chi^2 = & \left(\hat{J}_i^{\text{m}} - \hat{J}_i^{\text{p}}(\vec{x}) \right) C_{\text{exp}}^{-1} \left(\hat{J}_i^{\text{m}} - \hat{J}_i^{\text{p}}(\vec{x}) \right)^T \\ & + \left(\Gamma^{\text{m}} - \Gamma^{\text{p}}(V_{cb}, \vec{x}) \right)^2 / \sigma(\Gamma^{\text{m}})^2 \\ & + \left(h_X^{\text{LQCD}} - h_X^{\text{p}}(\vec{x}) \right) C_{\text{LQCD}}^{-1} \left(h_X^{\text{LQCD}} - h_X^{\text{p}}(\vec{x}) \right), \quad (4) \end{aligned}$$

which compares the measured (predicted) normalized angular coefficients $\Delta\hat{J}_i^{\text{m(p)}}$ in bins of w . The quantity $\Gamma^{\text{m(p)}}$ represents the predicted (externally measured) absolute rate. The predicted rate is a function of the form factor coefficients \vec{x} and $|V_{cb}|$, taking $m_B = 5.28 \text{ GeV}/c^2$, $m_{D^*} = 2.01 \text{ GeV}/c^2$, and $m_e = m_\mu = 0$. The parameters h_{A_1} , R_1 , R_2 are used for the predicted (LQCD) form factors $h_X^{\text{p(LQCD)}}$ and the form factors are evaluated at the w values provided by the lattice QCD predictions [19–21]. The three available lattice QCD predictions are used simultaneously. The covariance matrix C_{exp} (C_{LQCD}) corresponds to the experimental (lattice) data. We perform a nested hypothesis test [23] to determine the number of BGL coefficients required to describe the data, resulting in the choice $a = 3$, $b = 3$, $c = 2$, which are the number of free expansion coefficients for the BGL g , f , \mathcal{F}

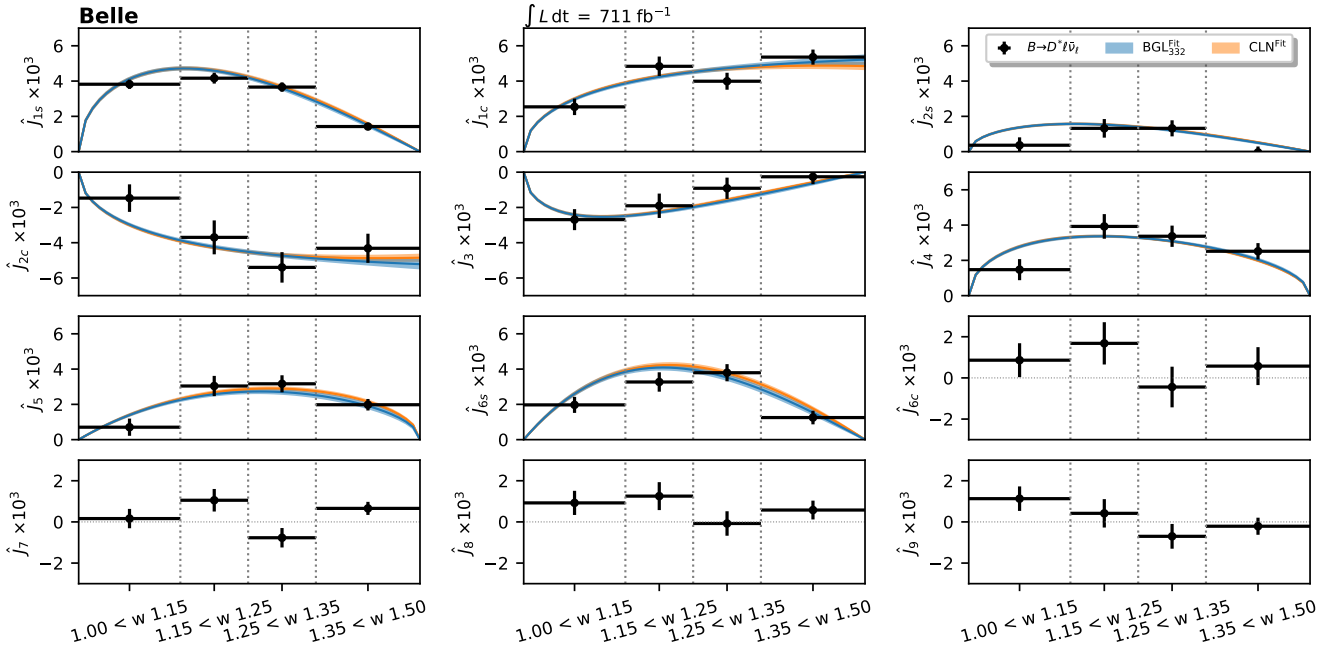


FIG. 1. The data points correspond to the averaged central values of the four measured normalized angular coefficients described in the text, with the uncertainties including statistical and systematic uncertainties. The vertical dotted lines indicate the binning in w . The blue (orange) curves correspond to the BGL₃₃₂ (CLN) fit described in the text, with the 1σ uncertainty band. The angular coefficients J_{6c} , J_7 , J_8 , J_9 are not fitted, and expected to be zero in the SM.

form factors, respectively. The p -values for the BGL₃₃₂ and CLN fits are 0.75 and 0.39, respectively. The fitted angular coefficients are shown in Fig. 1. The resulting form factors, together with the lattice data used in the fit, are shown in Fig. 2 [24]. We find consistent values for the CKM matrix element $|V_{cb}|$ for both form factor parameterizations:

$$|V_{cb}| = (41.0 \pm 0.3 \pm 0.4 \pm 0.5) \times 10^{-3} \text{ (BGL}_{332}\text{)},$$

$$|V_{cb}| = (40.9 \pm 0.3 \pm 0.4 \pm 0.4) \times 10^{-3} \text{ (CLN)},$$

where the first uncertainty is from the measured data, the second uncertainty is from the external branching fraction, and the third uncertainty is from the LQCD inputs.

The lepton forward-backward asymmetry A_{FB} and the D^* longitudinal polarization fraction $F_L(D^*)$ are straightforwardly calculated [25] from the measured angular coefficients within their corresponding w bins. The S_i observables in Ref. [26] are directly proportional to the angular coefficients $S_i \propto \hat{J}_i$ and are discussed further in the supplemental material. These observables can be used to test lepton flavor universality between electrons and muons via, e.g. $\Delta A_{\text{FB}} = A_{\text{FB}}^\mu - A_{\text{FB}}^e$ to search for new physics effects. We observe no significant deviation from the SM expectation and quantify the compatibility of each observable with the SM expectation in Table I. The corresponding lepton flavor universality observables are displayed in Fig. 3.

TABLE I. Compatibility of the lepton flavor universality observables with the SM expectation. The $\Delta X = X^\mu - X^e$ are the observables testing the lepton flavor universal by calculating the difference between the decays with muons and electrons.

Observable	χ^2 / ndf	p -value
ΔA_{FB}	1.7 / 4	0.79
$\Delta F_L(D^*)$	2.3 / 4	0.67
$\Delta \hat{J}_{1s}$	5.3 / 4	0.26
$\Delta \hat{J}_{1c}$	4.2 / 4	0.38
$\Delta \hat{J}_{2s}$	4.6 / 4	0.33
$\Delta \hat{J}_{2c}$	5.0 / 4	0.28
$\Delta \hat{J}_3$	7.4 / 4	0.12
$\Delta \hat{J}_4$	2.5 / 4	0.64
$\Delta \hat{J}_5$	4.8 / 4	0.31
$\Delta \hat{J}_{6s}$	2.1 / 4	0.72
$\Delta \hat{J}_{6c}$	1.1 / 4	0.89
$\Delta \hat{J}_7$	1.6 / 4	0.81
$\Delta \hat{J}_8$	3.3 / 4	0.51
$\Delta \hat{J}_9$	4.6 / 4	0.33
$\Delta \hat{J}_i$	41 / 48	0.76

In summary, we present the first complete measurement of the angular coefficients \hat{J}_i in bins of w describing the full differential decay distribution of $\bar{B} \rightarrow D^* \ell \bar{\nu}_\ell$ ($\ell = e, \mu$), probing both \bar{B}^0 and B^- modes. In total, we measure the partial rates in 4×144 distinct phase-space regions to extract the $4 \times 12 \hat{J}_i$ coefficients, with full sta-

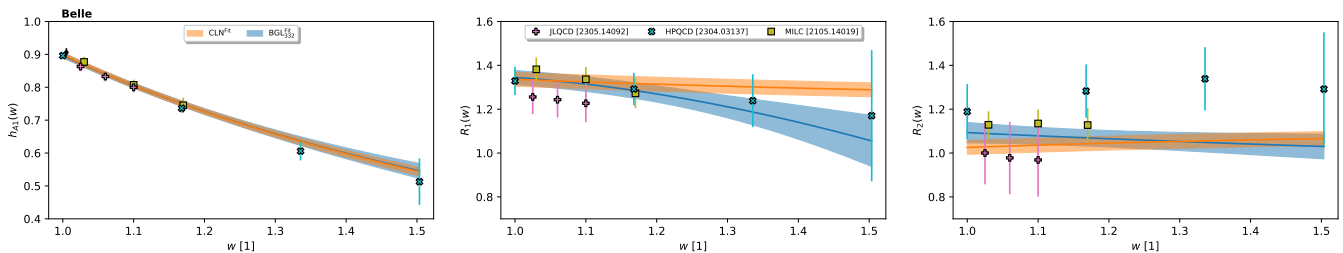


FIG. 2. The blue (orange) band corresponds to our form factor fits using the BGL_{332} (CLN) parameterizations with the beyond zero-recoil lattice predictions by (olive square) MILC [19], (cyan cross) HPQCD [20], and (pink plus) JLQCD [21] as input.

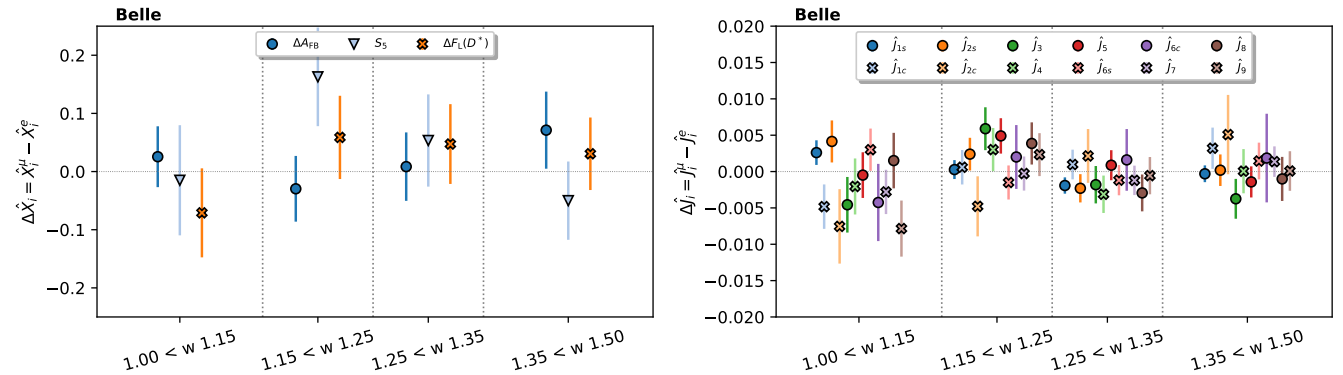


FIG. 3. The results of the lepton flavor universality test described in the text. The $\Delta X = X^\mu - X^e$ are the observables testing the lepton flavor universal by calculating the difference between the decays with muons and electrons. $\Delta S_5 \propto \Delta J_5$ is shown since a new physics signal should show up simultaneously in ΔA_{FB} and ΔS_5 . These asymmetries are expected to be approximately zero in the SM.

tistical and systematic correlations, allowing the simultaneous analysis of all measured angular coefficients. The measured coefficients encode the full angular information of the $\bar{B} \rightarrow D^* \ell \bar{\nu}_\ell$ decay, providing a more comprehensive set of observables than the one-dimensional partial rates of w , $\cos \theta_\ell$, $\cos \theta_V$, and χ measured in Refs. [3, 15].

The measured angular coefficients are analyzed to determine $|V_{cb}|$ using the beyond zero-recoil lattice calculations by the MILC, HPQCD, and JLQCD collaborations and the world average of the $\bar{B} \rightarrow D^* \ell \bar{\nu}_\ell$ branching fraction and B -meson lifetimes. We find $|V_{cb}| = (41.0 \pm 0.7) \times 10^{-3}$ in the BGL parameterization. The origin of the upward shift of $|V_{cb}|$ with respect to Ref. [3] is caused by the shift of $\mathcal{F}(1) = 0.895 \pm 0.007$ in the average of the new lattice results, and the smaller slope of the form factor compared to previous results. The resulting p -value of the fit is 75% and the value of $|V_{cb}|$ is in agreement with the fit of the one-dimensional partial rates determined from the same data set. The obtained values of $|V_{cb}|$ are compatible with the determinations using the CLN parameterization. These results are also in agreement with the two currently most precise determinations of $|V_{cb}|$ from inclusive $B \rightarrow X_c \ell \bar{\nu}_\ell$ measurements relying on heavy quark effective theory [27, 28]. Our results are in agreement with those determined from

partial rates [3], which uses the same dataset. A summary of our measurement of $|V_{cb}|$, together with other determinations, is shown in Fig. 4.

The measured angular coefficients are tested for lepton flavor universality violation, and no deviation from the SM expectation is observed. The numerical values, and full covariance matrices of the measured observables have been made available on HEPData.

ACKNOWLEDGMENTS

This work, based on data collected using the Belle detector, which was operated until June 2010, was supported by the Ministry of Education, Culture, Sports, Science, and Technology (MEXT) of Japan, the Japan Society for the Promotion of Science (JSPS), and the Tau-Lepton Physics Research Center of Nagoya University; the Australian Research Council including grants DP210101900, DP210102831, DE220100462, LE210100098, LE230100085; Austrian Federal Ministry of Education, Science and Research (FWF) and FWF Austrian Science Fund No. P 31361-N36; National Key R&D Program of China under Contract No. 2022YFA1601903, National Natural Science Foun-

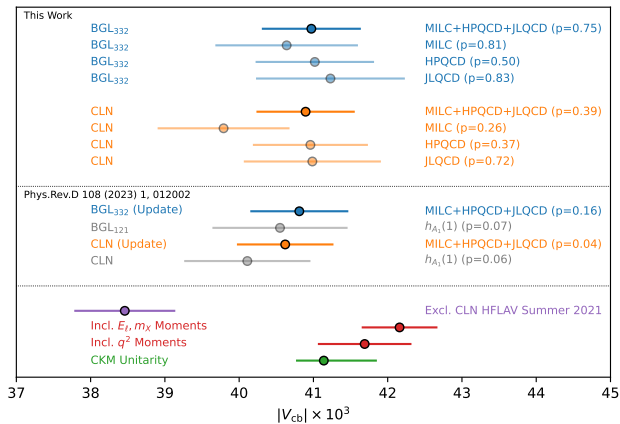


FIG. 4. The results of the $|V_{cb}|$ determination described in the text with other previous determinations. The top section shows the results of the analysis presented in this manuscript. The middle section shows the results in Ref. [3], where we have updated the fit with beyond zero-recoil lattice data. The bottom section shows the HVLAV [29] world average of $|V_{cb}|$, the $|V_{cb}|$ determinations from inclusive decays [27, 28], and $|V_{cb}|$ determination from CKM unitarity. The BGL and CLN labels indicate the form factor parameterization used to determine $|V_{cb}|$. The lattice QCD inputs are MILC [19], HPQCD [20], JLQCD [21]. Numbers in parentheses show goodness-of-fit p -values for the corresponding fits.

dation of China and research grants No. 11575017, No. 11761141009, No. 11705209, No. 11975076, No. 12135005, No. 12150004, No. 12161141008, and No. 12175041, and Shandong Provincial Natural Science Foundation Project ZR2022JQ02; the Czech Science Foundation Grant No. 22-18469S; Horizon 2020 ERC Advanced Grant No. 884719 and ERC Starting Grant No. 947006 “InterLeptons” (European Union); the Carl Zeiss Foundation, the Deutsche Forschungsgemeinschaft, the Excellence Cluster Universe, and the VolkswagenStiftung; the Department of Atomic Energy (Project Identification No. RTI 4002), the Department of Science and Technology of

India, and the UPES (India) SEED finding programs Nos. UPES/R&D-SEED-INFRA/17052023/01 and UPES/R&D-SOE/20062022/06; the Istituto Nazionale di Fisica Nucleare of Italy; National Research Foundation (NRF) of Korea Grant Nos. 2016R1D1A1B02012900, 2018R1A2B3003643, 2018R1A6A1A06024970, RS2022-00197659, 2019R1I1A3A01058933, 2021R1A6A1A-03043957, 2021R1F1A1060423, 2021R1F1A1064008, 2022R1A2C1003993; Radiation Science Research Institute, Foreign Large-size Research Facility Application Supporting project, the Global Science Experimental Data Hub Center of the Korea Institute of Science and Technology Information and KREONET/GLORIAD; the Polish Ministry of Science and Higher Education and the National Science Center; the Ministry of Science and Higher Education of the Russian Federation, Agreement 14.W03.31.0026, and the HSE University Basic Research Program, Moscow; University of Tabuk research grants S-1440-0321, S-0256-1438, and S-0280-1439 (Saudi Arabia); the Slovenian Research Agency Grant Nos. J1-9124 and P1-0135; Ikerbasque, Basque Foundation for Science, and the State Agency for Research of the Spanish Ministry of Science and Innovation through Grant No. PID2022-136510NB-C33 (Spain); the Swiss National Science Foundation; the Ministry of Education and the National Science and Technology Council of Taiwan; and the United States Department of Energy and the National Science Foundation. These acknowledgements are not to be interpreted as an endorsement of any statement made by any of our institutes, funding agencies, governments, or their representatives.

We thank the KEKB group for the excellent operation of the accelerator; the KEK cryogenics group for the efficient operation of the solenoid; and the KEK computer group and the Pacific Northwest National Laboratory (PNNL) Environmental Molecular Sciences Laboratory (EMSL) computing group for strong computing support; and the National Institute of Informatics, and Science Information NETwork 6 (SINET6) for valuable network support.

-
- [1] S. Kurokawa and E. Kikutani, Nucl. Instr. and Meth. **A499**, 1 (2003), and other papers included in this Volume; T. Abe *et al.*, Prog. Theor. Exp. Phys. **2013**, 03A001 (2013) and references therein.
- [2] A. Abashian *et al.*, Nucl. Instrum. Meth. **A479**, 117 (2002), also see detector section in J. Brodzicka *et al.*, Prog. Theor. Exp. Phys. **2012**, 04D001 (2012).
- [3] M. T. Prim *et al.* (Belle), Phys. Rev. D **108**, 012002 (2023), arXiv:2301.07529 [hep-ex].
- [4] A. Sirlin, Nucl. Phys. **B196**, 83 (1982).
- [5] F. U. Bernlochner, Z. Ligeti, and S. Turczyk, Phys. Rev. D **90**, 094003 (2014), arXiv:1408.2516 [hep-ph].
- [6] Charge conjugation is implicit throughout this Letter.
- [7] R. L. Workman *et al.* (Particle Data Group), PTEP **2022**, 083C01 (2022).
- [8] H. Nakano *et al.* (Belle), Phys. Rev. D **97**, 092003 (2018), arXiv:1803.07774 [hep-ex].
- [9] J. F. Krohn *et al.* (Belle-II analysis software Group), Nucl. Instrum. Meth. A **976**, 164269 (2020), arXiv:1901.11198 [hep-ex].
- [10] T. Keck *et al.*, Comput. Softw. Big Sci. **3**, 6 (2019), arXiv:1807.08680 [hep-ex].
- [11] Ed.: A. Bevan, B. Golob, T. Mannel, S. Prell, and B. Yabsley, Eur. Phys. J. C **74**, 3026 (2014), Chapter 9: Background Suppression for B Decays, arXiv:1406.6311 [hep-ex].
- [12] The Fox-Wolfram moments were introduced in G. C. Fox and S. Wolfram, Phys. Rev. Lett. **41**, 1581 (1978). The

- modified Fox-Wolfram moments (SFW) used by Belle are described in K. Abe *et al.* (Belle Collaboration), Phys. Rev. Lett. **87**, 101801 (2001) and K. Abe *et al.* (Belle Collaboration), Phys. Lett. **B 511**, 151 (2001). We use the same set of the moments described in these references.
- [13] D. M. Asner *et al.* (CLEO Collaboration), Phys. Rev. **D 53**, 1039 (1996).
- [14] T. Keck, Comput. Softw. Big Sci. **1**, 2 (2017).
- [15] E. Waheed *et al.* (Belle), Phys. Rev. D **100**, 052007 (2019), [Erratum: Phys.Rev.D 103, 079901 (2021)], arXiv:1809.03290 [hep-ex].
- [16] I. Caprini, L. Lellouch, and M. Neubert, Nucl. Phys. B **530**, 153 (1998), arXiv:hep-ph/9712417.
- [17] C. G. Boyd, B. Grinstein, and R. F. Lebed, Nucl. Phys. B **461**, 493 (1996), arXiv:hep-ph/9508211.
- [18] C. G. Boyd, B. Grinstein, and R. F. Lebed, Phys. Rev. D **56**, 6895 (1997), arXiv:hep-ph/9705252.
- [19] A. Bazavov *et al.* (Fermilab Lattice, MILC), Eur. Phys. J. C **82**, 1141 (2022), arXiv:2105.14019 [hep-lat].
- [20] J. Harrison and C. T. H. Davies, (2023), arXiv:2304.03137 [hep-lat].
- [21] Y. Aoki, B. Colquhoun, H. Fukaya, S. Hashimoto, T. Kaneko, R. Kellermann, J. Koponen, and E. Kou (JLQCD), (2023), arXiv:2306.05657 [hep-lat].
- [22] Y. Amhis *et al.*, (2022), arXiv:2206.07501 [hep-ex].
- [23] F. U. Bernlochner, Z. Ligeti, and D. J. Robinson, Phys. Rev. D **100**, 013005 (2019), arXiv:1902.09553 [hep-ph].
- [24] Tabulated results and further details can be found in the supplemental material.
- [25] For more details, including necessary relations, refer to the supplemental material.
- [26] C. Bobeth, M. Bordone, N. Gubernari, M. Jung, and D. van Dyk, Eur. Phys. J. C **81**, 984 (2021), arXiv:2104.02094 [hep-ph].
- [27] M. Bordone, B. Capdevila, and P. Gambino, Phys. Lett. B **822**, 136679 (2021), arXiv:2107.00604 [hep-ph].
- [28] F. Bernlochner, M. Fael, K. Olschewsky, E. Persson, R. van Tonder, K. K. Vos, and M. Welsch, (2022), arXiv:2205.10274 [hep-ph].
- [29] Y. Amhis *et al.* (HFLAV), (2022), arXiv:2206.07501 [hep-ex].

Supplemental Material

I. DEFINITIONS OF THE ANGULAR COEFFICIENTS

In the SM the angular coefficients for $B \rightarrow D^* \ell \bar{\nu}_\ell$ with $D^* \rightarrow D\pi$ can be written in terms of the helicity amplitudes:

$$\begin{aligned}
J_{1s} &= F \left(\frac{1}{2} (H_+^2 + H_-^2) (m_\ell^2 + 3q^2) \right), \\
J_{1c} &= F (2(2m_\ell^2 H_t^2 + H_0^2 (m_\ell^2 + q^2))), \\
J_{2s} &= F \left(\frac{1}{2} (H_+^2 + H_-^2) (q^2 - m_\ell^2) \right), \\
J_{2c} &= F (2H_0^2 (m_\ell^2 - q^2)), \\
J_3 &= F (2H_+ H_- (m_\ell^2 - q^2)), \\
J_4 &= -F (H_0 (H_+ + H_-) (m_\ell^2 - q^2)), \\
J_5 &= F (-2(H_+ + H_-) H_t m_\ell^2 - 2H_0 (H_+ - H_-) q^2), \\
J_{6s} &= -F (2(H_+^2 - H_-^2) q^2), \\
J_{6c} &= -F (-8H_0 H_t m_\ell^2), \\
J_7 &= 0, \\
J_8 &= 0, \\
J_9 &= 0,
\end{aligned} \tag{5}$$

with $F = (2/m_B^3)(3p_{D^*})/(128 \times 2^4 m_B^2)$.

II. RELATIONS BETWEEN COMMON OBSERVABLES AND ANGULAR COEFFICIENTS

The forward-backward asymmetry and the longitudinal polarization fractions are

$$A_{\text{FB}} = \frac{3}{2} \frac{(J_{6c} + 2J_{6s})}{3J_{1c} - J_{2c} + 2(3J_{1s} - J_{2s})}, \tag{6}$$

$$F_L(D^*) = \frac{(3J_{1c} - J_{2c})}{3J_{1c} - J_{2c} + 2(3J_{1s} - J_{2s})}, \tag{7}$$

$$\tag{8}$$

where the denominator is only a normalization factor.

The S_i observables in the text are directly proportional to the angular coefficients $S_i \propto \hat{J}_i$. The relations are

$$S_3 = \frac{1}{\pi} \frac{4J_3}{3J_{1c} - J_{2c} + 2(3J_{1s} - J_{2s})}, \tag{9}$$

$$S_5 = \frac{3J_5}{3J_{1c} - J_{2c} + 2(3J_{1s} - J_{2s})}, \tag{10}$$

$$S_7 = \frac{3J_7}{3J_{1c} - J_{2c} + 2(3J_{1s} - J_{2s})}, \tag{11}$$

$$S_9 = \frac{1}{\pi} \frac{4J_9}{3J_{1c} - J_{2c} + 2(3J_{1s} - J_{2s})}, \tag{12}$$

$$\tag{13}$$

where the denominator is only a normalization factor. Thus $S_i \propto J_i$. The numerical values are shown in Tab. ?? . The correlations are provided in the HEPData repository.

TABLE II. Observables calculated from the average J_i of the four measured decay modes.

w bin	A_{FB}	$F_L(D^*)$	S_3	S_5	S_7	S_9
$1.00 < w < 1.15$	0.23 ± 0.03	0.29 ± 0.04	-0.11 ± 0.02	0.07 ± 0.05	0.02 ± 0.05	0.05 ± 0.02
$1.15 < w < 1.25$	0.30 ± 0.03	0.45 ± 0.04	-0.06 ± 0.02	0.23 ± 0.04	0.08 ± 0.04	0.01 ± 0.02
$1.25 < w < 1.35$	0.29 ± 0.03	0.47 ± 0.03	-0.03 ± 0.02	0.26 ± 0.04	-0.06 ± 0.04	-0.02 ± 0.02
$1.35 < w < 1.50$	0.16 ± 0.03	0.70 ± 0.03	-0.01 ± 0.02	0.20 ± 0.03	0.07 ± 0.03	-0.01 ± 0.02

III. SYSTEMATICS

The uncertainties of the angular coefficients are shown for their individual components in Tab. ???. The dominant systematic uncertainty is the limited MC statistics.

IV. $|V_{cb}|$ FITTING DETAILS

We translate the available beyond zero-recoil lattice QCD prediction for the $B \rightarrow D^*$ form factors into the h_{A_1} , R_1 , and R_2 representation using the relations

$$R_1 = \frac{h_V}{h_{A_1}}, \quad R_2 = \frac{h_{A_3} + r_{D^*} h_{A_2}}{h_{A_1}} \quad (14)$$

with $r^* = m_{D^*}/m_B$, and

$$h_{A_1} = \frac{f}{m_B \sqrt{r^*} (w+1)}, \quad h_V = g m_B \sqrt{r^*}, \quad (15)$$

$$h_{A_1} (w - r^* - (w-1) R_2) = \frac{F_1}{m_B^2 \sqrt{r^*} (w+1)},$$

The coefficients for the fit described in the main text are shown in Table VII for the BGL fit, and Table VIII for the CLN fit. We also investigate the B^0 and B^+ decay modes independently. We find consistent values for $|V_{cb}|$: $|V_{cb}|_{\text{CLN}}^{B^0} = 40.9 \pm 0.7$, $|V_{cb}|_{\text{BGL}}^{B^0} = 40.8 \pm 0.7$, $|V_{cb}|_{\text{CLN}}^{B^+} = 41.3 \pm 0.7$, $|V_{cb}|_{\text{BGL}}^{B^+} = 41.3 \pm 0.7$. Here, we have used the same number of BGL coefficients as the nominal fit.

TABLE III. Uncertainties in % for the $\bar{B}^0 \rightarrow D^* e \bar{\nu}_e$ channel

J_i	w bin	total M_{miss}^2 fit		Unfolding and Acceptance									
		FF($B \rightarrow D^* \ell \nu$)	$\mathcal{B}(D \rightarrow X)$	MC stat.	$\epsilon(\pi_{\text{slow}})$	$\epsilon(\text{LID})$	$\epsilon(\pi^0)$	$\epsilon(\text{Tracking})$	$\epsilon(K_S^0)$	FEI	Shape		
J_{1s}	[1.00, 1.15]	23.21	22.32	0.87	0.87	6.18	0.84	0.16	0.18	0.08	0.01	0.42	
	[1.15, 1.25]	14.53	14.02	0.53	0.15	3.72	0.23	0.11	0.11	0.00	0.01	0.48	
	[1.25, 1.35]	11.65	11.17	1.23	0.39	3.04	0.29	0.06	0.10	0.02	0.01	0.09	
	[1.35, 1.51]	10.34	9.97	1.09	0.42	2.46	0.22	0.07	0.08	0.02	0.01	0.27	
J_{1c}	[1.00, 1.15]	40.45	38.54	1.01	0.51	12.18	0.77	0.20	0.00	0.01	0.02	0.66	
	[1.15, 1.25]	27.00	26.14	1.26	0.23	6.58	0.30	0.09	0.17	0.01	0.04	0.73	
	[1.25, 1.35]	22.34	21.74	1.20	0.25	4.96	0.23	0.23	0.01	0.03	0.00	0.25	
	[1.35, 1.51]	23.25	22.52	2.23	0.53	5.29	0.44	0.47	0.08	0.07	0.01	0.12	
J_{2s}	[1.00, 1.15]	41.57	39.97	0.60	0.66	11.38	0.16	0.25	0.07	0.04	0.02	0.34	
	[1.15, 1.25]	25.08	24.16	1.02	0.34	6.62	0.11	0.06	0.08	0.03	0.02	0.11	
	[1.25, 1.35]	19.69	18.79	1.31	0.29	5.72	0.12	0.08	0.05	0.01	0.01	0.36	
	[1.35, 1.51]	18.96	18.38	1.54	0.14	4.40	0.07	0.08	0.02	0.01	0.01	0.14	
J_{2c}	[1.00, 1.15]	70.83	67.77	1.19	0.95	20.51	0.35	0.07	0.04	0.03	0.02	1.11	
	[1.15, 1.25]	46.84	44.80	1.95	0.68	13.51	0.24	0.11	0.09	0.06	0.03	0.17	
	[1.25, 1.35]	39.22	38.15	1.41	0.65	8.92	0.35	0.19	0.01	0.00	0.03	0.58	
	[1.35, 1.51]	45.04	43.74	1.92	0.58	10.46	0.44	0.74	0.06	0.02	0.02	1.23	
J_3	[1.00, 1.15]	52.83	51.04	1.10	0.32	13.56	0.19	0.09	0.00	0.02	0.05	1.02	
	[1.15, 1.25]	29.46	28.49	1.15	0.38	7.33	0.21	0.07	0.06	0.01	0.02	0.99	
	[1.25, 1.35]	24.57	23.76	1.47	0.43	6.00	0.13	0.15	0.11	0.00	0.01	0.85	
	[1.35, 1.51]	23.50	22.84	1.77	0.33	5.20	0.07	0.04	0.05	0.01	0.01	0.12	
J_4	[1.00, 1.15]	55.54	53.48	0.39	0.49	14.93	0.32	0.11	0.06	0.00	0.02	1.18	
	[1.15, 1.25]	30.94	29.98	0.65	0.39	7.58	0.30	0.07	0.08	0.00	0.01	0.88	
	[1.25, 1.35]	24.83	23.97	0.72	0.35	6.44	0.26	0.17	0.02	0.04	0.01	0.22	
	[1.35, 1.51]	25.86	25.07	1.37	0.71	5.96	0.37	0.08	0.20	0.03	0.01	1.48	
J_5	[1.00, 1.15]	43.22	41.89	1.31	0.43	10.54	0.43	0.19	0.03	0.01	0.02	0.06	
	[1.15, 1.25]	25.23	24.38	1.32	0.31	6.35	0.12	0.27	0.02	0.01	0.01	0.42	
	[1.25, 1.35]	20.16	19.32	1.23	0.30	5.57	0.12	0.16	0.00	0.03	0.01	0.39	
	[1.35, 1.51]	18.13	17.56	1.72	0.54	4.10	0.32	0.14	0.07	0.04	0.01	0.52	
J_{6s}	[1.00, 1.15]	40.96	39.58	1.76	0.84	10.30	0.59	0.28	0.22	0.05	0.02	0.66	
	[1.15, 1.25]	24.63	23.90	1.31	0.22	5.67	0.24	0.47	0.08	0.01	0.02	1.03	
	[1.25, 1.35]	20.01	19.15	1.38	0.46	5.51	0.32	0.54	0.16	0.05	0.01	0.78	
	[1.35, 1.51]	21.57	20.91	1.44	0.44	5.08	0.18	0.50	0.05	0.03	0.03	0.07	
J_{6c}	[1.00, 1.15]	66.26	63.94	0.74	0.52	17.36	0.29	0.19	0.20	0.00	0.02	0.37	
	[1.15, 1.25]	46.82	45.56	0.87	0.85	10.59	0.20	0.90	0.42	0.03	0.03	1.34	
	[1.25, 1.35]	43.08	41.63	1.10	0.38	10.86	0.26	1.44	0.09	0.04	0.02	1.18	
	[1.35, 1.51]	52.87	51.48	1.07	0.37	11.69	0.16	2.48	0.03	0.02	0.04	0.47	
J_7	[1.00, 1.15]	43.07	41.77	0.17	0.46	10.48	0.09	0.07	0.15	0.01	0.01	0.65	
	[1.15, 1.25]	24.53	23.81	0.33	0.20	5.88	0.12	0.05	0.05	0.02	0.01	0.23	
	[1.25, 1.35]	19.79	19.21	0.15	0.22	4.64	0.09	0.02	0.02	0.01	0.02	1.09	
	[1.35, 1.51]	17.80	17.31	0.18	0.16	4.16	0.08	0.01	0.01	0.00	0.01	0.11	
J_8	[1.00, 1.15]	54.76	52.77	0.17	0.68	14.61	0.15	0.03	0.06	0.04	0.01	0.50	
	[1.15, 1.25]	31.10	29.86	0.18	0.30	8.68	0.14	0.06	0.07	0.00	0.03	0.02	
	[1.25, 1.35]	24.98	23.99	0.24	0.42	6.92	0.13	0.09	0.06	0.04	0.01	0.53	
	[1.35, 1.51]	26.06	25.23	0.31	0.37	6.52	0.14	0.05	0.09	0.03	0.01	0.03	
J_9	[1.00, 1.15]	55.59	54.12	0.59	0.84	12.64	0.63	0.04	0.31	0.00	0.05	0.41	
	[1.15, 1.25]	30.19	29.00	0.22	0.26	8.38	0.10	0.02	0.01	0.00	0.01	0.33	
	[1.25, 1.35]	25.00	24.22	0.10	0.23	6.17	0.10	0.01	0.09	0.01	0.02	0.31	
	[1.35, 1.51]	23.36	22.94	0.12	0.21	4.37	0.05	0.06	0.03	0.02	0.01	0.24	

TABLE IV. Uncertainties in % for the $\bar{B}^0 \rightarrow D^* \mu \bar{\nu}_\mu$ channel

J_i	w bin	total M_{miss}^2 fit		Unfolding and Acceptance									
		FF($B \rightarrow D^* \ell \nu$)	$\mathcal{B}(D \rightarrow X)$	MC stat.	$\epsilon(\pi_{\text{slow}})$	$\epsilon(\text{LID})$	$\epsilon(\pi^0)$	$\epsilon(\text{Tracking})$	$\epsilon(K_S^0)$	FEI	Shape		
J_{1s}	[1.00, 1.15)	23.53	22.42	1.19	1.32	6.82	0.99	0.05	0.28		0.12	0.03	0.57
	[1.15, 1.25)	13.42	12.81	0.62	0.13	3.93	0.20	0.05	0.01		0.01	0.01	0.02
	[1.25, 1.35)	10.89	10.38	1.17	0.43	3.04	0.29	0.14	0.10		0.04	0.01	0.00
	[1.35, 1.51)	10.26	9.85	1.19	0.20	2.56	0.20	0.09	0.02		0.02	0.01	0.22
J_{1c}	[1.00, 1.15)	35.81	34.39	0.84	0.30	9.92	0.90	0.23	0.06		0.01	0.01	0.16
	[1.15, 1.25)	20.48	19.63	1.06	0.26	5.72	0.22	0.02	0.05		0.01	0.01	0.19
	[1.25, 1.35)	20.05	19.27	1.06	0.24	5.41	0.20	0.12	0.07		0.03	0.00	0.03
	[1.35, 1.51)	28.93	27.76	2.40	1.16	7.64	0.65	0.25	0.40		0.08	0.03	0.07
J_{2s}	[1.00, 1.15)	43.84	42.06	0.64	0.60	12.32	0.63	0.18	0.03		0.07	0.03	0.22
	[1.15, 1.25)	23.59	22.61	0.96	0.20	6.62	0.11	0.11	0.02		0.03	0.01	0.24
	[1.25, 1.35)	18.82	17.91	1.06	0.23	5.65	0.14	0.19	0.03		0.02	0.01	0.14
	[1.35, 1.51)	19.83	19.08	1.74	0.17	5.13	0.11	0.04	0.07		0.02	0.01	0.12
J_{2c}	[1.00, 1.15)	62.30	60.17	0.55	0.96	16.08	0.65	0.07	0.07		0.09	0.03	0.46
	[1.15, 1.25)	37.32	36.30	1.84	0.27	8.49	0.21	0.27	0.07		0.07	0.03	0.20
	[1.25, 1.35)	36.58	35.48	1.18	0.45	8.81	0.36	0.11	0.06		0.07	0.02	0.18
	[1.35, 1.51)	55.71	53.90	2.11	0.51	13.78	0.29	0.14	0.16		0.05	0.02	1.91
J_3	[1.00, 1.15)	49.51	47.65	1.20	1.12	13.25	0.42	0.15	0.45		0.03	0.02	1.49
	[1.15, 1.25)	29.74	28.80	1.07	0.37	7.30	0.20	0.04	0.06		0.05	0.02	0.66
	[1.25, 1.35)	23.65	22.81	1.52	0.36	5.99	0.20	0.03	0.05		0.03	0.01	0.64
	[1.35, 1.51)	25.05	24.28	1.63	0.26	5.94	0.16	0.10	0.04		0.00	0.01	0.22
J_4	[1.00, 1.15)	48.88	47.60	0.45	0.72	10.88	0.49	0.28	0.17		0.01	0.02	2.03
	[1.15, 1.25)	29.96	28.90	0.98	0.53	7.82	0.26	0.10	0.15		0.03	0.01	0.07
	[1.25, 1.35)	24.76	23.66	0.65	0.48	7.21	0.31	0.20	0.12		0.06	0.02	0.56
	[1.35, 1.51)	28.43	27.52	1.09	0.59	6.99	0.35	0.20	0.17		0.04	0.01	0.60
J_5	[1.00, 1.15)	40.88	39.50	1.39	0.53	10.41	0.37	0.06	0.01		0.01	0.03	0.62
	[1.15, 1.25)	24.57	23.45	1.58	0.44	7.08	0.14	0.18	0.05		0.04	0.02	0.95
	[1.25, 1.35)	19.77	18.83	1.37	0.34	5.84	0.36	0.08	0.09		0.03	0.02	0.39
	[1.35, 1.51)	19.41	18.88	1.27	0.29	4.30	0.23	0.08	0.02		0.01	0.01	0.13
J_{6s}	[1.00, 1.15)	39.72	38.19	1.78	1.20	10.62	1.10	0.18	0.31		0.10	0.02	0.58
	[1.15, 1.25)	25.38	24.34	1.18	0.28	7.07	0.21	0.03	0.02		0.00	0.01	0.66
	[1.25, 1.35)	20.07	19.35	1.28	0.44	5.12	0.31	0.22	0.08		0.05	0.02	0.19
	[1.35, 1.51)	24.35	23.79	1.60	0.64	4.90	0.20	0.14	0.07		0.03	0.00	0.02
J_{6c}	[1.00, 1.15)	65.84	63.82	0.73	0.50	16.13	0.48	0.04	0.25		0.00	0.02	0.13
	[1.15, 1.25)	43.21	41.57	1.00	0.41	11.69	0.19	0.09	0.12		0.01	0.01	1.27
	[1.25, 1.35)	41.82	40.79	1.12	0.21	9.12	0.18	0.07	0.02		0.06	0.02	0.43
	[1.35, 1.51)	61.00	59.72	1.29	0.80	12.24	0.22	0.12	0.07		0.01	0.02	1.61
J_7	[1.00, 1.15)	40.48	39.05	0.15	0.36	10.66	0.20	0.09	0.02		0.02	0.03	0.63
	[1.15, 1.25)	23.87	23.12	0.20	0.18	5.81	0.12	0.11	0.03		0.03	0.01	1.26
	[1.25, 1.35)	18.96	18.22	0.28	0.27	5.19	0.13	0.02	0.02		0.01	0.00	0.82
	[1.35, 1.51)	19.06	18.51	0.13	0.10	4.52	0.07	0.05	0.04		0.00	0.01	0.39
J_8	[1.00, 1.15)	50.17	48.05	0.26	0.50	14.37	0.53	0.08	0.19		0.01	0.02	1.25
	[1.15, 1.25)	29.21	28.15	0.51	0.24	7.71	0.17	0.03	0.00		0.02	0.01	1.04
	[1.25, 1.35)	23.51	22.59	0.23	0.31	6.41	0.10	0.02	0.12		0.00	0.01	1.09
	[1.35, 1.51)	27.80	26.94	0.06	0.20	6.85	0.05	0.14	0.00		0.00	0.01	0.28
J_9	[1.00, 1.15)	51.08	49.14	0.25	0.64	13.73	0.53	0.03	0.01		0.07	0.09	2.10
	[1.15, 1.25)	29.01	28.04	0.58	0.33	7.36	0.16	0.03	0.11		0.01	0.02	0.60
	[1.25, 1.35)	23.92	23.13	0.23	0.34	6.05	0.13	0.06	0.14		0.02	0.02	0.29
	[1.35, 1.51)	24.85	24.09	0.04	0.25	6.10	0.11	0.02	0.00		0.02	0.01	0.15

TABLE V. Uncertainties in % for the $\bar{B}^+ \rightarrow D^* e \bar{\nu}_e$ channel

J_i	w bin	total M_{miss}^2 fit		Unfolding and Acceptance									
		FF($B \rightarrow D^* \ell \nu$)	$\mathcal{B}(D \rightarrow X)$	MC stat.	$\epsilon(\pi_{\text{slow}})$	$\epsilon(\text{LID})$	$\epsilon(\pi^0)$	$\epsilon(\text{Tracking})$	$\epsilon(K_S^0)$	FEI	Shape		
J_{1s}	[1.00, 1.15]	15.39	14.79	1.07	0.24	4.08	0.40	0.20	0.01	0.01	0.01	0.01	0.43
	[1.15, 1.25]	12.77	12.35	0.56	0.15	3.17	0.44	0.04	0.01	0.01	0.01	0.01	0.01
	[1.25, 1.35]	11.83	11.41	1.13	0.11	2.89	0.43	0.07	0.03	0.00	0.00	0.00	0.10
	[1.35, 1.51]	13.19	12.88	0.96	0.15	2.62	0.35	0.07	0.01	0.01	0.01	0.01	0.40
J_{1c}	[1.00, 1.15]	29.25	28.28	0.91	0.21	7.20	1.00	0.17	0.04	0.00	0.01	0.01	1.34
	[1.15, 1.25]	23.67	22.88	1.05	0.18	5.89	0.75	0.09	0.06	0.01	0.01	0.01	0.09
	[1.25, 1.35]	19.28	18.82	1.03	0.18	3.99	0.42	0.22	0.06	0.01	0.01	0.01	0.32
	[1.35, 1.51]	30.08	29.52	1.96	0.26	5.35	0.29	0.52	0.03	0.00	0.01	0.01	0.50
J_{2s}	[1.00, 1.15]	25.89	25.01	0.41	0.36	6.65	0.13	0.15	0.04	0.00	0.00	0.00	0.65
	[1.15, 1.25]	22.28	21.59	0.98	0.42	5.39	0.11	0.09	0.03	0.01	0.00	0.00	0.02
	[1.25, 1.35]	20.89	20.10	1.27	0.25	5.52	0.11	0.05	0.02	0.01	0.01	0.01	0.02
	[1.35, 1.51]	25.60	25.06	1.33	0.29	4.95	0.15	0.11	0.00	0.01	0.01	0.01	0.97
J_{2c}	[1.00, 1.15]	48.37	46.80	1.02	0.65	12.09	0.37	0.13	0.09	0.02	0.02	0.02	1.36
	[1.15, 1.25]	41.41	40.49	1.61	0.64	8.49	0.22	0.25	0.09	0.02	0.01	0.01	0.07
	[1.25, 1.35]	36.08	34.98	1.27	0.38	8.73	0.27	0.15	0.04	0.01	0.01	0.01	0.57
	[1.35, 1.51]	60.89	59.81	2.49	0.68	10.97	0.38	0.73	0.01	0.06	0.02	0.02	1.68
J_3	[1.00, 1.15]	34.53	33.69	1.14	0.40	7.45	0.26	0.27	0.00	0.02	0.01	0.01	0.53
	[1.15, 1.25]	30.71	29.92	1.18	0.23	6.85	0.15	0.04	0.08	0.06	0.02	0.02	0.12
	[1.25, 1.35]	28.58	27.75	1.39	0.22	6.69	0.08	0.07	0.15	0.04	0.00	0.00	0.16
	[1.35, 1.51]	33.15	32.56	1.63	0.21	6.01	0.11	0.03	0.01	0.02	0.02	0.02	0.33
J_4	[1.00, 1.15]	33.48	32.66	0.46	0.40	7.16	0.48	0.14	0.08	0.04	0.03	0.03	1.54
	[1.15, 1.25]	30.59	29.82	0.68	0.58	6.72	0.23	0.03	0.09	0.06	0.01	0.01	0.19
	[1.25, 1.35]	27.63	26.85	0.74	0.46	6.44	0.22	0.07	0.03	0.00	0.01	0.01	0.80
	[1.35, 1.51]	36.23	35.39	1.24	0.49	7.54	0.12	0.39	0.08	0.01	0.00	0.00	1.00
J_5	[1.00, 1.15]	27.28	26.47	1.43	0.13	6.43	0.21	0.12	0.00	0.02	0.01	0.01	0.12
	[1.15, 1.25]	25.01	24.29	1.31	0.08	5.81	0.09	0.34	0.04	0.02	0.00	0.00	0.20
	[1.25, 1.35]	22.30	21.63	1.21	0.31	5.27	0.17	0.20	0.03	0.01	0.00	0.00	0.18
	[1.35, 1.51]	25.54	24.93	1.39	0.23	5.36	0.09	0.26	0.02	0.00	0.01	0.01	0.09
J_{6s}	[1.00, 1.15]	25.91	25.01	2.14	0.27	6.39	0.26	0.32	0.12	0.03	0.01	0.01	0.44
	[1.15, 1.25]	23.67	22.81	1.27	0.17	6.16	0.39	0.58	0.01	0.02	0.01	0.01	0.42
	[1.25, 1.35]	21.67	21.12	1.17	0.16	4.68	0.35	0.52	0.01	0.01	0.01	0.01	0.21
	[1.35, 1.51]	28.27	27.62	1.34	0.35	5.79	0.19	0.58	0.00	0.04	0.02	0.02	0.49
J_{6c}	[1.00, 1.15]	49.20	47.55	0.92	0.49	12.57	0.79	0.19	0.19	0.05	0.01	0.01	0.60
	[1.15, 1.25]	44.76	43.46	0.82	0.16	10.66	0.56	0.49	0.03	0.01	0.02	0.02	0.19
	[1.25, 1.35]	41.60	40.50	1.11	0.27	9.34	0.34	1.11	0.09	0.02	0.01	0.01	0.21
	[1.35, 1.51]	63.43	62.16	1.32	0.75	12.34	0.17	2.21	0.05	0.08	0.02	0.02	0.37
J_7	[1.00, 1.15]	27.21	26.48	0.19	0.17	6.26	0.17	0.14	0.05	0.05	0.02	0.02	0.33
	[1.15, 1.25]	24.31	23.60	0.28	0.39	5.80	0.11	0.08	0.05	0.03	0.01	0.01	0.21
	[1.25, 1.35]	21.71	21.23	0.26	0.17	4.50	0.16	0.15	0.06	0.01	0.01	0.01	0.40
	[1.35, 1.51]	25.07	24.56	0.53	0.16	4.97	0.16	0.15	0.04	0.00	0.02	0.02	0.17
J_8	[1.00, 1.15]	34.28	33.26	0.20	0.43	8.21	0.19	0.05	0.09	0.03	0.03	0.03	0.85
	[1.15, 1.25]	30.07	29.33	0.31	0.26	6.55	0.14	0.04	0.05	0.02	0.01	0.01	1.18
	[1.25, 1.35]	27.11	26.49	0.08	0.44	5.71	0.20	0.11	0.00	0.02	0.01	0.01	0.61
	[1.35, 1.51]	35.30	34.60	0.12	0.42	6.95	0.18	0.12	0.02	0.03	0.02	0.02	0.57
J_9	[1.00, 1.15]	34.17	33.15	0.38	0.36	8.24	0.32	0.13	0.02	0.05	0.04	0.04	0.09
	[1.15, 1.25]	30.88	30.02	0.14	0.14	7.22	0.19	0.03	0.06	0.01	0.01	0.01	0.65
	[1.25, 1.35]	27.15	26.61	0.17	0.26	5.36	0.16	0.14	0.01	0.00	0.01	0.01	0.11
	[1.35, 1.51]	32.87	32.29	0.29	0.27	6.14	0.11	0.01	0.00	0.01	0.02	0.02	0.31

TABLE VI. Uncertainties in % for the $\bar{B}^+ \rightarrow D^* \mu \bar{\nu}_\mu$ channel

J_i	w bin	total M_{miss}^2 fit		Unfolding and Acceptance									
		FF($B \rightarrow D^* \ell \nu$)	$\mathcal{B}(D \rightarrow X)$	MC stat.	$\epsilon(\pi_{\text{slow}})$	$\epsilon(\text{LID})$	$\epsilon(\pi^0)$	$\epsilon(\text{Tracking})$	$\epsilon(K_S^0)$	FEI	Shape		
J_{1s}	[1.00, 1.15)	12.91	12.21	1.18	0.19	4.01	0.44	0.06	0.06	0.00	0.02	0.18	
	[1.15, 1.25)	12.93	12.42	0.62	0.15	3.49	0.45	0.02	0.01	0.02	0.01	0.05	
	[1.25, 1.35)	11.06	10.67	0.81	0.12	2.80	0.35	0.06	0.02	0.00	0.01	0.06	
	[1.35, 1.51)	13.91	13.48	1.07	0.32	3.15	0.35	0.02	0.05	0.01	0.01	0.72	
J_{1c}	[1.00, 1.15)	23.29	22.32	0.99	0.37	6.51	0.89	0.05	0.09	0.02	0.01	0.04	
	[1.15, 1.25)	25.39	24.29	1.33	0.42	7.25	0.66	0.02	0.00	0.06	0.01	0.00	
	[1.25, 1.35)	21.98	21.18	0.92	0.14	5.75	0.44	0.14	0.02	0.01	0.01	0.18	
	[1.35, 1.51)	34.53	33.70	2.06	0.99	7.07	0.38	0.11	0.13	0.05	0.02	1.09	
J_{2s}	[1.00, 1.15)	22.07	21.08	0.42	0.38	6.50	0.31	0.05	0.10	0.02	0.03	0.18	
	[1.15, 1.25)	21.25	20.38	1.00	0.19	5.92	0.18	0.05	0.00	0.00	0.02	0.31	
	[1.25, 1.35)	19.44	18.85	0.76	0.27	4.70	0.08	0.07	0.02	0.01	0.01	0.08	
	[1.35, 1.51)	25.89	25.05	1.50	0.48	6.31	0.11	0.02	0.02	0.00	0.02	0.70	
J_{2c}	[1.00, 1.15)	39.79	38.41	1.04	0.81	10.29	0.60	0.17	0.06	0.02	0.04	0.06	
	[1.15, 1.25)	41.77	39.77	2.01	0.34	12.60	0.16	0.20	0.03	0.04	0.04	0.18	
	[1.25, 1.35)	39.00	37.80	1.17	0.44	9.53	0.18	0.19	0.06	0.03	0.02	0.49	
	[1.35, 1.51)	64.25	62.65	2.16	1.30	13.89	0.35	0.38	0.11	0.04	0.03	1.94	
J_3	[1.00, 1.15)	29.51	28.33	1.32	0.35	8.08	0.30	0.11	0.08	0.06	0.01	0.99	
	[1.15, 1.25)	28.99	28.05	1.35	0.43	7.18	0.17	0.11	0.17	0.00	0.02	0.32	
	[1.25, 1.35)	27.11	26.23	1.30	0.27	6.63	0.16	0.03	0.06	0.01	0.01	1.13	
	[1.35, 1.51)	33.10	32.39	1.37	0.43	6.68	0.13	0.02	0.03	0.00	0.02	0.38	
J_4	[1.00, 1.15)	31.48	30.24	0.43	0.48	8.69	0.30	0.05	0.10	0.02	0.05	0.43	
	[1.15, 1.25)	29.33	28.26	1.06	0.44	7.75	0.34	0.03	0.04	0.03	0.02	0.06	
	[1.25, 1.35)	27.09	26.30	0.12	0.21	6.45	0.15	0.07	0.00	0.02	0.01	0.76	
	[1.35, 1.51)	37.61	36.63	0.93	0.37	8.46	0.21	0.10	0.00	0.01	0.02	0.25	
J_5	[1.00, 1.15)	25.19	24.01	1.43	0.46	7.45	0.18	0.08	0.10	0.00	0.03	0.40	
	[1.15, 1.25)	23.80	22.91	1.71	0.23	6.19	0.19	0.21	0.10	0.00	0.01	0.12	
	[1.25, 1.35)	22.01	21.29	0.95	0.23	5.47	0.12	0.02	0.04	0.00	0.01	0.48	
	[1.35, 1.51)	27.09	26.26	1.03	0.20	6.57	0.21	0.06	0.03	0.02	0.01	0.34	
J_{6s}	[1.00, 1.15)	22.73	21.76	2.08	0.53	6.18	0.27	0.19	0.02	0.03	0.03	0.33	
	[1.15, 1.25)	21.92	21.04	1.28	0.39	5.99	0.44	0.06	0.06	0.01	0.02	0.14	
	[1.25, 1.35)	22.39	21.89	1.04	0.09	4.59	0.35	0.07	0.01	0.00	0.01	0.07	
	[1.35, 1.51)	29.98	29.42	1.42	0.19	5.58	0.27	0.02	0.07	0.01	0.01	0.21	
J_{6c}	[1.00, 1.15)	42.62	41.23	0.68	0.97	10.71	0.55	0.05	0.02	0.06	0.02	0.69	
	[1.15, 1.25)	43.40	41.88	0.84	0.78	11.26	0.56	0.18	0.12	0.01	0.03	0.99	
	[1.25, 1.35)	46.03	45.08	0.93	0.26	9.26	0.50	0.09	0.13	0.01	0.03	0.42	
	[1.35, 1.51)	72.42	71.07	1.20	0.35	13.86	0.34	0.12	0.08	0.00	0.04	0.45	
J_7	[1.00, 1.15)	23.68	22.83	0.10	0.36	6.26	0.19	0.09	0.13	0.02	0.01	0.55	
	[1.15, 1.25)	22.11	21.44	0.27	0.13	5.31	0.11	0.02	0.01	0.04	0.02	0.76	
	[1.25, 1.35)	21.72	20.84	0.06	0.13	6.12	0.15	0.06	0.02	0.00	0.00	0.01	
	[1.35, 1.51)	25.41	24.70	0.46	0.31	5.93	0.16	0.02	0.03	0.03	0.01	0.06	
J_8	[1.00, 1.15)	29.02	28.33	0.18	0.34	6.26	0.22	0.09	0.00	0.04	0.01	0.35	
	[1.15, 1.25)	27.20	26.15	0.41	0.26	7.41	0.11	0.04	0.06	0.04	0.00	0.94	
	[1.25, 1.35)	27.14	26.35	0.14	0.19	6.50	0.13	0.08	0.02	0.03	0.01	0.31	
	[1.35, 1.51)	36.51	35.61	0.32	0.54	8.04	0.19	0.03	0.01	0.03	0.01	0.40	
J_9	[1.00, 1.15)	30.06	29.09	0.19	0.77	7.55	0.19	0.10	0.04	0.09	0.01	0.15	
	[1.15, 1.25)	28.55	27.41	0.27	0.20	7.94	0.20	0.05	0.09	0.01	0.02	0.75	
	[1.25, 1.35)	27.68	26.80	0.07	0.27	6.92	0.09	0.01	0.00	0.02	0.01	0.32	
	[1.35, 1.51)	32.80	32.17	0.14	0.26	6.40	0.11	0.05	0.04	0.02	0.01	0.29	

TABLE VII. The fitted coefficients for the BGL fit described in the text.

	Value	Correlation									
$a_0 \times 10^2$	2.68 ± 0.06	1.00	0.03	-0.11	0.17	0.00	-0.02	0.08	-0.04	-0.19	
$a_1 \times 10^2$	-2.65 ± 2.35	0.03	1.00	-0.67	-0.01	0.17	-0.03	0.09	-0.03	-0.10	
$a_2 \times 10^2$	-145.18 ± 87.35	-0.11	-0.67	1.00	0.03	-0.02	-0.03	0.01	-0.05	-0.03	
$b_0 \times 10^2$	1.30 ± 0.01	0.17	-0.01	0.03	1.00	-0.02	0.02	0.02	-0.03	-0.50	
$b_1 \times 10^2$	1.30 ± 0.66	0.00	0.17	-0.02	-0.02	1.00	-0.66	0.59	-0.46	-0.28	
$b_2 \times 10^2$	-11.50 ± 22.40	-0.02	-0.03	-0.03	0.02	-0.66	1.00	-0.45	0.40	-0.04	
$c_1 \times 10^2$	-0.25 ± 0.16	0.08	0.09	0.01	0.02	0.59	-0.45	1.00	-0.82	-0.32	
$c_2 \times 10^2$	0.78 ± 3.29	-0.04	-0.03	-0.05	-0.03	-0.46	0.40	-0.82	1.00	0.05	
$ V_{cb} \times 10^3$	40.97 ± 0.67	-0.19	-0.10	-0.03	-0.50	-0.28	-0.04	-0.32	0.05	1.00	

TABLE VIII. The fitted coefficients for the CLN fit described in the text.

	Value	Correlation					
$h_{A_1}(1)$	0.90 ± 0.01	1.00	0.02	-0.18	-0.04	-0.50	
ρ^2	1.13 ± 0.04	0.02	1.00	0.05	-0.48	0.40	
$R_1(1)$	1.34 ± 0.03	-0.18	0.05	1.00	-0.10	-0.02	
$R_2(1)$	1.03 ± 0.03	-0.04	-0.48	-0.10	1.00	0.17	
$ V_{cb} \times 10^3$	40.89 ± 0.66	-0.50	0.40	-0.02	0.17	1.00	